Can machine learning predict friction from third body morphology?

Alizée Bouchot, Amandine Ferrieux, Johan Debayle, Guilhem Mollon, Sylvie Descartes

Can Machine Learning Predict Friction from Third Body Morphology?

Bouchot Alizée [a,b,*], Ferrieux Amandine[a], Debayle Johan[c], Mollon Guilhem[a,*], Descartes Sylvie[a,*]

[a]*Univ Lyon, INSA Lyon, CNRS, LaMCoS, UMR5259, Villeurbanne, 69621, France*
[b]*Univ Lyon, ECAM LaSalle, LabECAM, 40 Montée Saint Barthélémy, Lyon Cedex 05, 69321, France*
[c]*Mines Saint-Etienne, CNRS, UMR 5307 LGF, Centre SPIN, Saint-Etienne, F - 42023, France*

* Corresponding authors: a.bouchot-madrignac@ecam.fr (Alizée Bouchot), guilhem.mollon@insa-lyon.fr (Guilhem Mollon), sylvie.descartes@insa-lyon.fr (Sylvie Descartes)

Abstract
This work proposes to lay the foundations for building an efficient database that is representative of the morphology of the third body, with the aim of understanding whether it is possible to predict the local friction coefficient from it, using Machine Learning (ML). Five different databases (including morphological properties of ejected wear particles and textural properties of on-track third-body) are constructed, and a Random Forest (RF) machine learning algorithm is implemented. Results show that an algorithm trained on third body morphological features can provide a fairly accurate prediction of the local value of the friction coefficient in a variety of tribological situations, with an average error close to 0.14 for measured values ranging between 0.1 and 1.2.

Keywords: Dry friction, Experiment, Third Body, Morphology, Machine Learning

1. Introduction

Following the work of Peter Jost in 1966 [1], the scientific community became increasingly interested in the costs generated by friction and wear. Numerous theories were developed to address this issue, in particular Maurice Godet's third body theory [2], which was later formalized by Yves Berthier [3], taking the form of a tribological circuit in which the third body flows into the contact. The tribological history and state of the contact can thus be described by observing the interface and interpreting the various third body flows. The accuracy of this operation depends on the tribologist's judgement and experience, and is therefore highly subjective by nature. This is why the use of image analysis techniques has become widespread in order to study and characterize the morphology of wear particles with the aim of linking it to wear mechanisms or experimental conditions (see in particular [4]–[9]). Studying the morphology of wear particles gives access to their shape and size and can help to understand what type of wear led to their production. In most studies, the particles are collected and observed by microscopy (optical and/or electron). The resulting images are then processed and segmented. From the resulting binary images, size and shape metrics can be extracted and processed manually or automatically. This approach however presents the risk to disrupt the structure of the third body agglomerates, and to disregard its spatial patterns on the track. The work proposed here therefore focuses on dry contact, with the wear particles remaining on their production substrate and the list of their descriptors being supplemented by texture

descriptors characterizing the morphology of the friction track. The idea here is no longer to classify the particles into categories corresponding to their production mode, but to predict the local value of the friction coefficient measured experimentally. It is indeed well-known that, in many engineering situations, the instantaneous friction coefficient can be highly fluctuating and rather unpredictable, contrary to, say a time- or space-averaged friction for which more repeatability is expected. For this purpose, this work describes the use of a supervised machine learning algorithm that works as follows: a learning system will be 'fed' with labelled observations to enable it to create and update its prediction model of the local friction coefficient based on local morphological quantities. The use of such algorithms requires the construction of labelled databases, made up of labels and features, and the focus of the present work is therefore mostly put on the design and construction of the most relevant morphological database for friction prediction.

As mentioned above, a model combines a labelled database and an algorithm. An important tribological literature exists on the choice of the best ML algorithm in a given framework ([10], [11]), sometimes with limited guarantee that its performances can be transposed to a different framework. In view of the work carried out on the subject, the choice of algorithm does not seem to be the most discriminating factor in view of the performance measured ([12], [13]), and the quality of the training database plays an (at least) equally important role in the construction of the model [12]. Furthermore, no state-of-the-art protocol exists yet for the constitution of a morphological database for tribological purposes, and we do not have any *a priori* knowledge on what its content should be in order to maximize prediction abilities [13]. Thus, the aim of the work presented here is to focus on the appropriate choice and construction of the database for the considered problem. Regarding the choice of the algorithm, Deep Learning is primarily a prediction tool, and its informative power is still limited (although gaining popularity for tribological applications [14]). A classical Machine Learning (ML) algorithm has therefore been chosen among the numerous existing ML algorithms in order to gain knowledge on the system at stake, before resorting to more powerful solutions in future studies. Detailed reasons are given in section 3.

The major contributions of this work are solid proofs that (i) a direct quantitative link between third body morphology and instantaneous friction can be established for prediction purposes, and that (ii) Machine Learning algorithms are appropriate tools for such a task. The manuscript has the following structure: Section 2 presents the acquisition and processing of experimental data; Section 3 then describes the construction and evaluation of the databases; In section 4, we discuss the generalization of these databases; Section 5 concludes the work.

2. Experimental methodology: data acquisition and processing

2.1. Experimental set up

To produce experimental data, a pin-on-disc tribometer, presented on Figure 1, is used. It consists of a rotating a low-carbon alloy steel disk and a pin, both made of 35CrNiMo16 steel, fixed to an arm that allows 2 degrees of freedom, namely the translation tangential to the movement (along y) and the vertical translation (along z). A vertical dead load is applied on the pin, and the system is equipped with a force sensor to measure the tangential force, and thus determine the coefficient of friction and an eddy-current sensor serving as a lap counter. A transparent casing allows to monitor and control the gaseous environment of the experiment. Initial surfaces are extracted using a Zygo Zegage PRO non-contact optical profiler. Prior to analyses and sliding tests, the as-received samples surfaces are cleaned by ultrasound and chemically in an ethyl-acetate bath for 5 min. This cleaning eliminates residual pollution due to specimen handling and machining. Then rinsing is done in an ethanol bath for 5 min. The surface roughness of the initial state is Sa = 0.207 µ*m.*

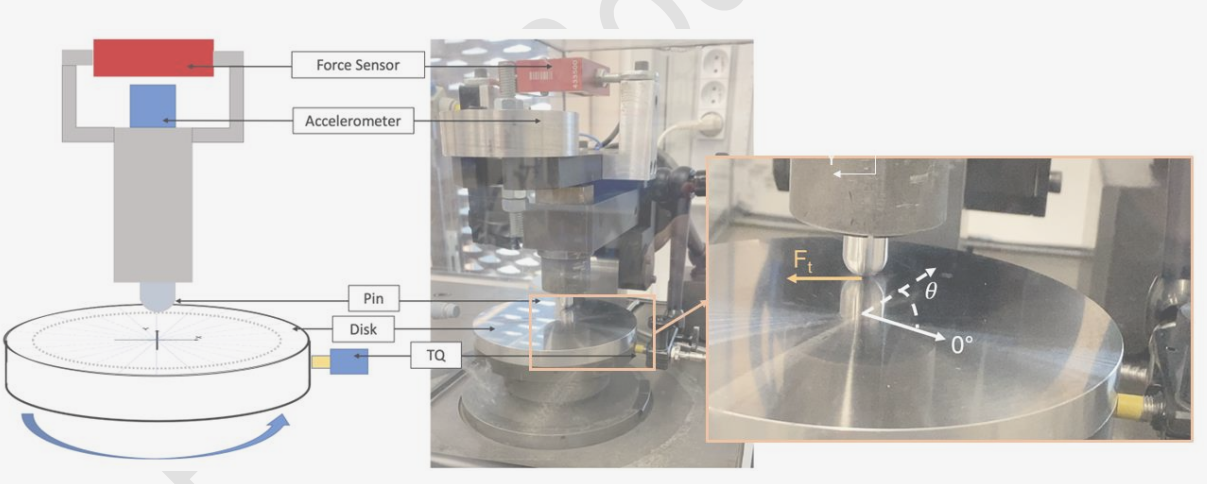

Figure 1: Pin on disk tribometer

A total of 14 tests are performed, as presented in Table 1, where several experimental parameters are varied: thickness of the disk, track radius, sliding distance, and gaseous environment (ambient air or argon), in order to product a panel of third bodies of varied morphology. The axial load (10 N) and the sliding velocity (6.26 mm/s) are kept constants for all tests, and a new pin is employed in each experiment. Temperature and relative humidity are measured at the beginning of each test. Tests are assigned the designations of D*n*P*m*, where *n* is the disc number and *m* is the pin number. These tests can be grouped into four categories. The first category (D10P20 to D10P23) corresponds to a set of long-distance tests in free atmosphere or Argon (Alpha gas 1 quality), performed

on a disk of 10 mm of thickness. The second one (D11P24 to D11P27) corresponds to a set of short distance tests performed on a 10 mm disk in free atmosphere. The third one (D12P28 to D12P31) corresponds to tests performed on a 15 mm-thick disk, at various sliding distances in Argon and free atmosphere. The change in disc thickness necessitates modifying the height of the arm holding the pin by adding a shim to the tribometer. Modifying the thickness of the disk may induce slight changes in the dynamic response of the tribosystem [15], [16] thus possibly the friction. The last one (D17P42 and D151P43) corresponds to a set of additional tests performed in a free atmosphere on 10 and 15 mm thick disks.

Test D_nP_m	Thickness of the disk (mm)	Radius (mm)	Angular Speed (RPM)	Distance (m)	T (◦C)	RH (%)	Atm.
D10P20	10	27	2.22	12	19.4	<1%	Argon
D10P21	10	33	1.82	18	19.3	<1%	Argon
D10P22	10	39	1.53	12	20.3	43	Free
D10P23	10	45	1.33	18	22.8	42	Free
D11P24	10	27	2.22	1	20	37	Free
D11P25	10	33	1.82	2	20	37	Free
D11P26	10	39	1.53	3	20	37	Free
D11P27	10	45	1.33	6	21	37	Free
D12P28	15	27	2.22	7.46	20	<1%	Argon
D12P29	15	33	1.82	18	18.7	<1%	Argon
D12P30	15	39	1.53	6	18.2	38	Free
D12P31	15	45	1.33	18	18.2	38	Free
D17P42	10	45	1.33	25	18.9	29.9	Free
D151P43	15	45	1.33	25	20	31.4	Free

Table 1: Experimental conditions for tribological testing. (Where T is temperature, RH is relative humidity and Atm is atmosphere)

The aim of this work is to highlight the existence of correlations between friction and morphology of the third body, and to evaluate to what extent the value of the friction coefficient can be predicted from these morphological characteristics. It is therefore necessary to extract morphological data at several locations of each disc after tribological testing. To that extend, Scanning Electron microscopy (SEM) imaging is employed. As described in tribological literature [2], [17], the flows of material in a sliding system can be described using the tribological circuit. The first bodies, in contact, are in relative motion; the third body is formed at the sliding interface. The source flow, Q_s, represents the detachment of the material from the first body to become the third body; the internal flow Q_i describes the movement of the material along the interface; the ejection flow Q_e is the material ejected from the interface; the recirculation flow Q_r is the ejected material that has been reintroduced into the interface; and the wear flow Q_w is the material that has been permanently removed from the sliding

system. During this study, the morphology of the third body contributed to those different flows is studied, in order to establish what links, exist between the local state of the interface and the measured friction coefficient. It is possible to highlight the consequences of the flows Q_i and Q_w thanks to third body morphology observations by taking SEM images at selected locations every 15° on the sliding track. For each position, it is necessary to focus on three areas: The track center (corresponding to Q_i), and both sides of the track (corresponding to Q_w). Figure 2 illustrates these regions of interest (ROI), on the disk. Table 2 provides the SEM images acquisition conditions.

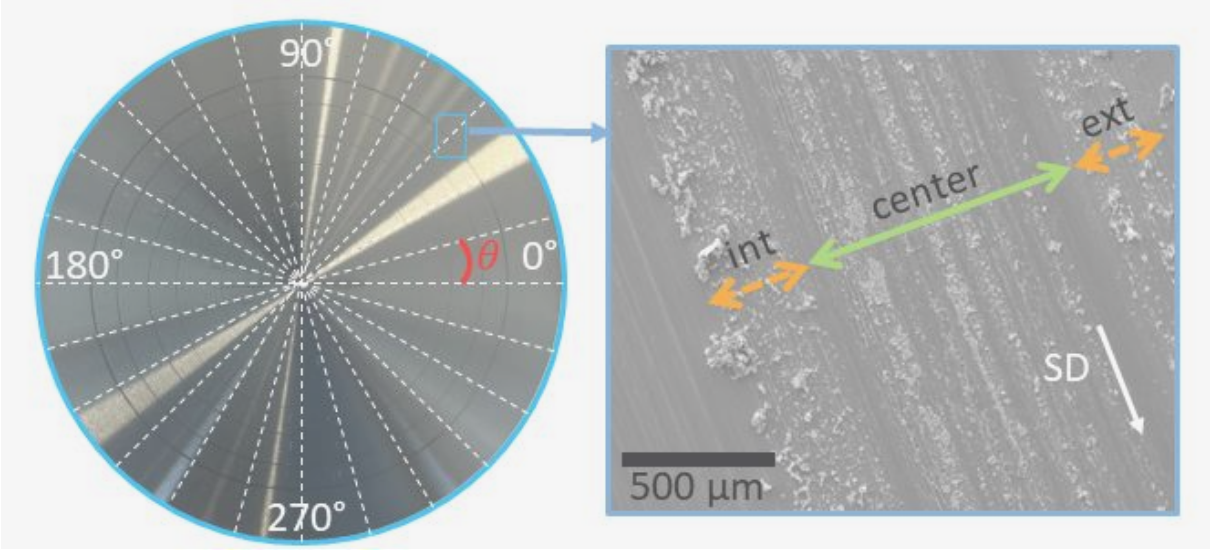

Figure 2: Localization of Region Of Interest (ROI) on disk. (SD = Sliding Direction).

SEM Parameters	Value
Detector	Everhart-Thornley (secondary electrons detection)
Dwell time (µs)	30
Resolution (px)	1024 x 884
Working distance (mm)	10
High voltage (kV)	20
Spot size	5 (i.e. beam current = 1.2nA)

Table 2 : SEM image acquisition conditions.

2.2 Tribological results

Figure 3 Provides a general view of the tribological results. In Figure 3a, the raw friction signal of the test D10P22 is provided for the whole test duration (about 30 minutes). This test is performed under ambient air on a total distance of about 12 m. The friction signal exhibits a large variability in time and appears considerably noisy.

However, periodic patterns are revealed by zooming in on just a few laps (Figure 3b), corresponding to successive passages on the same areas of the disc. Hence, friction data can be represented using a color scale map format (figure 3c), as a function of track angular position on the disc (horizontal x-axis) and number of sliding laps (vertical y-axis). Some very clear patterns do appear in this friction map. For example, a steady increase of the friction is observed in time, in every location of the disc, during the first ~25 laps, until a relative stabilization. During some time periods friction drops consistently everywhere on the disc during a couple of laps (around laps 10, 28, and 42, as highlighted by horizontal dotted lines). Such events are certainly related to temporary modifications of the pin surface/interface, since they happen concomitantly everywhere on the disc. Meanwhile, vertical patterns (around angles of 80° and 220° for example, as highlighted by vertical dotted lines) correspond to consistent friction drops every time the pin passes certain locations on the disc: these patterns are therefore related to some local properties of the disc at these locations.

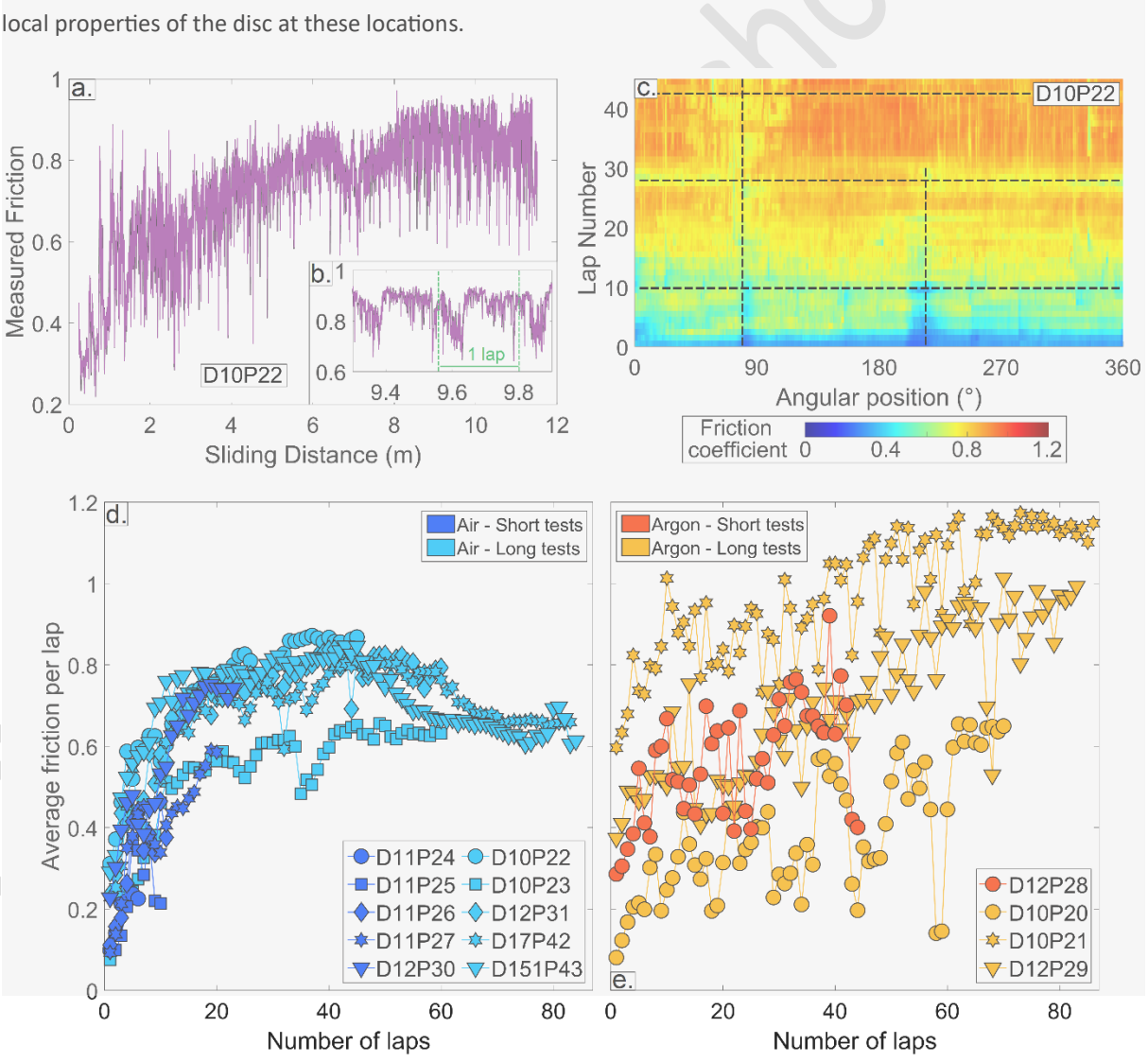

Figure 3: Tribological results; a. Raw friction signal for the test D10P22; b. Zoomed view on a few lap-periods of the same signal; c. Friction map in space (angular position) and time (number of laps), with dotted lines enhancing horizontal and

vertical patterns; d. Evolution of average coefficient of friction per lap, for the 10 tests performed in air; e. Evolution of average coefficient of friction per lap, for the 4 tests performed in argon

In order to provide an overview of the results of the 14 tests, Figures 3d and 3e show the evolution of the average friction coefficient per lap (i.e. per full rotation of the disc around its axis) as a function of the number of laps, in the case of the 14 tests (Table 1). Tests are plotted separately depending on their gaseous atmosphere, and a difference is made between short (less than 10 m of sliding) and long tests. For tests performed in ambient air (Figure 3d), a common trend can be observed, despite a certain variability between tests. In all cases, the initial averaged friction is low (between 0.1 and 0.3), and then rises steeply during the first 20-30 laps and more slowly until lap ~40. For the majority of long tests, it reaches a value close to 0.8, and then gently decreases to stabilize at around 0.65 after ~60 laps. The only exception is test D10P23, which does not reach the peak and 0.8 and instead directly converges towards an average value of 0.65. This value therefore seems to be a long-term stable value for the steel/steel contact, but it is important to keep in mind that this is an average value per lap, and that it hides local variations on each location of each disc. The cause of these variations, however, remains elusive, although some elements of understanding are provided in the remainder of the present work.

The four tests performed in argon (Figure 3e) are more difficult to interpret, because they provide quantitatively dissimilar results (albeit common trends). For the very first laps of these tests, average friction values as different as 0.1 and 0.6 are measured among the different tests. As the number of laps increases, one can observe a general increase of the friction coefficient for all cases, in a rather consistent manner: tests starting at a low friction end up lower than tests starting at a high friction. This increase is much more irregular than for the tests performed in air, with sudden drops and rapid recoveries of the average friction, typically during one or two laps. After about 60 laps, the drops are disappearing, and the tests reach what could be called stationary states, but with friction values as different as 0.6 and 1.1.

Whatever the case for which such a steady state is reached, a typical increase of about 0.5 before the first and the last lap is observed.

2.3 Third body features

Figure 3 highlights that the measured friction in all these steel-steel contact vary greatly, both in space and time. Since the materials of the bodies into contact are identical, these differences must be linked to the state of the

contact interface, and most primarily to the properties of the third body layer, i.e., the layer of matter separating the sliding surfaces. Many experimental and numerical studies [18]–[20] indeed showed that the flow regime and the rheology of this layer are one of the major factors controlling friction. This layer can be introduced on purpose but is most often a spontaneous by-product of the damaging of the contacting surfaces, as in the present study. Figure 4a provides for example a general view of a selected location on the track of the test D11P26, ran in ambient air, and stopped after 3 meters of sliding. As shown in Figures 4b, the central part of the track is 200-300 µm-wide and is covered by a limited but noticeable amount of (roughly micrometric) third body particles. Figure 4c shows that this is also the case on the ejection zones on both sides of the track. Generally, we observe a relatively granular third body, even powdery in the ejection zones and crushed in the central region. Figure 4d shows the friction map for this test, which indicates that the coefficient of friction has already started to evolve since the first lap, in concomitance with the appearance of the early third body layer observed in Figures 4a-c. The Figure 4e provides the friction signal for the last lap of the test, with instantaneous friction coefficients measured between 0.2 and 0.6. At the selected location shown in SEM views, the last recorded friction coefficient is close to 0.5. As confirmed by the friction map, this is a location of slightly higher friction than in the 90-180° region for example.

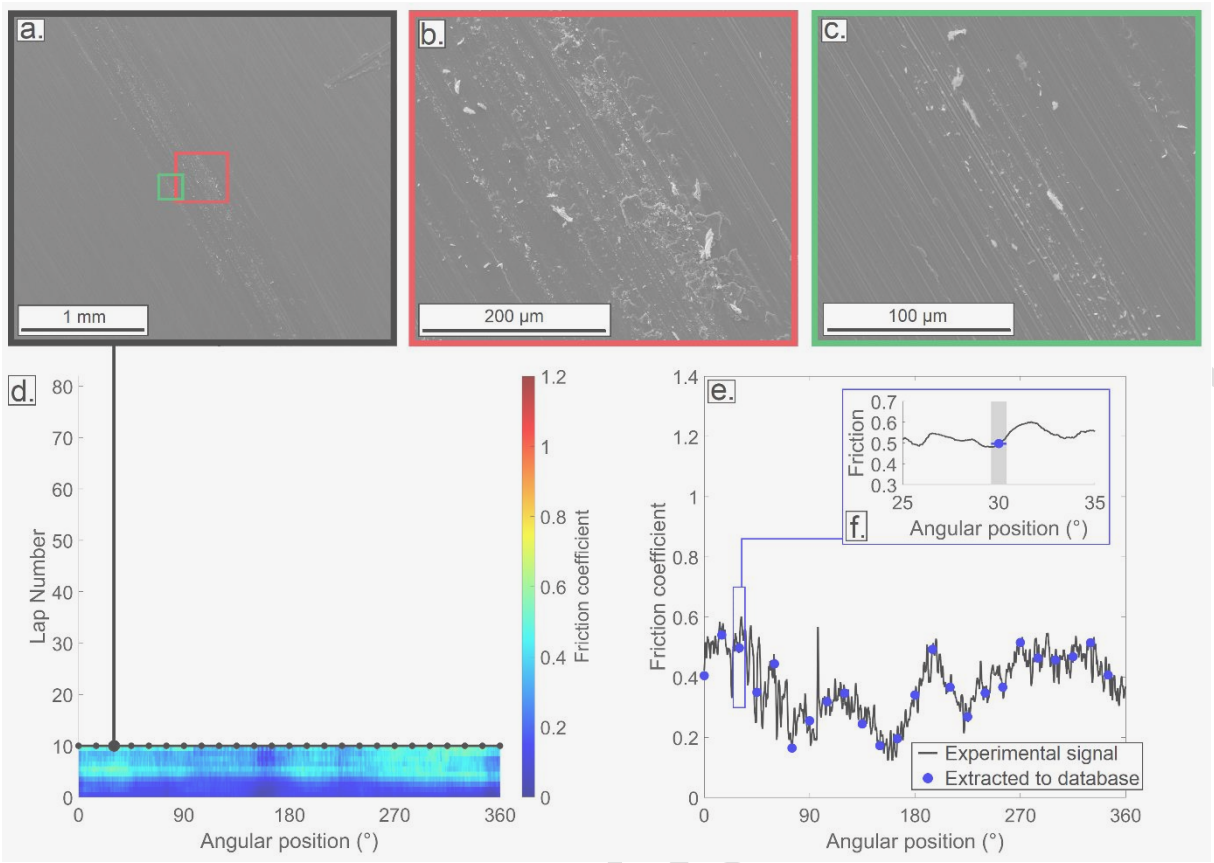

Figure 4: Local observations and measurements for a short test in air: D11P26. a. General view of the track after 10 laps at the angular position 30°; b. View of the centre of the track; c. View of the ejection zone (interior); d. Friction map with black dots indicating SEM observations (including a., b., c.); e. Friction signal during the last lap, with blue dots indicating SEM observation points extracted to the general database; f. Zoom on the friction averaging window (31 points with sampling frequency of 1000Hz) around angular position 30°

Figure 5a shows the final state of a selected location on the track of the test D12P31, which was running in ambient air until a final sliding distance of 18 meters. Detailed view of the track centre (internal flow) and of the track side (wear flow) are provided respectively in Figures 5b and 5c. These figures show that the track is now much wider (~1 mm) and covered with a much larger amount of powdery third body, both in the contact zone and in the ejection zone. This third body seems mildly cohesive and forms some apparently loose agglomerates. Following the nomenclature developed in [21], this may qualify as a granular accommodation regime. As shown in the friction map (Figure 5d), some initial heterogeneities of the disc (initial low friction regions at angular position 60° and 110°) seem to have been levelled after about 35 laps. A friction drop occurred on the whole track during laps 42-43 (probably because of a change in the pin surface, e.g., detachment of a large third body agglomerate, see [22] , but previous friction was quickly recovered. This is confirmed by the friction signal during the last lap (Figure 5e), which indicates a steady friction level close to 0.8 on the whole track, and a local value

close to 0.85 (Fig 5f) in the area depicted in Figure 5a-c. Comparing with Figure 4, it seems that, under ambient air, an increase in the quantity of third body correlates with an increase in friction, and also in friction stability.

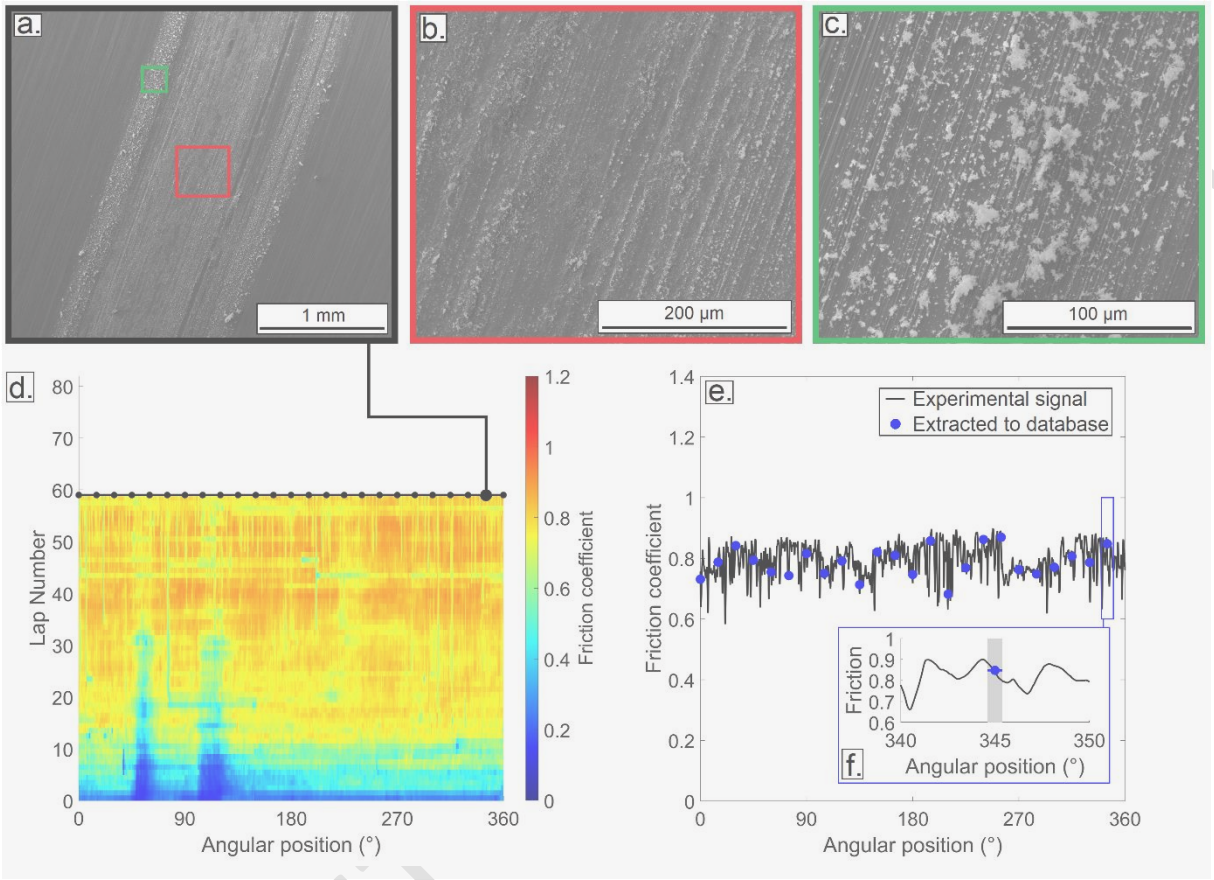

Figure 5: Local observations and measurements for a long test in air: D12P31. a. General view of the track after 60 laps at the angular position 345°; b. View of the centre of the track; c. View of the ejection zone (interior); d. Friction map with black dots indicating SEM observations (including a., b., c.); e. Friction signal during the last lap, with blue dots indicating SEM observation points extracted to the general database; f. Zoom on the friction averaging window around angular position 345°

Figure 6 is dedicated to test D12P29, performed in argon until a sliding distance of 18 meters, and depicts very different phenomena. As shown in Figure 6a-c, the sliding track is about 1.5 mm-wide, and is covered by a large amount of large (10-100 µm) third body agglomerates, which can also be observed in smaller quantity in the ejection zone. This third body therefore appears as cohesive, brittle-looking fragments that settle on the track and are cut into smaller flakes without spreading out very much laterally. The friction map provided in Figure 6d is characteristic of those obtained for each argon test of the present study and appears very different from those of ambient air tests. In contrast with the steady and general friction increase depicted in Figure 5d, this map is characterized by a general background of rather low friction (typically lower than 0.5) with very sudden events

during which friction increases above 1. During the first 25 laps, these events are rather rare and short-lived, but the get more and more frequent between 25 and 50 laps and ubiquitous after 50 laps. A very informative feature is the presence of stair-like patterns for some of these events (see e.g., in the 180° region around lap 30). A plausible hypothesis would be to relate these friction jumps to the trapping of large agglomerates of third body, such as the one depicted in Figure 6c. The stair-like patterns would therefore correspond to the pin capturing the agglomerate for a few centimetres of sliding, then releasing it behind and recapturing it at a later lap. This hypothesis is also consistent with the progressive build-up of a large collection of such agglomerates on the track, and with the fact that the period of generalized large friction (end of the test) is concomitant with the observation of a large amount of third body (Figure 6a). This type of flow regime was reproduced numerically [23], [24], and indeed led to larger friction coefficients than in the granular case. During the last lap (Figure 6f), the recorded friction is generally comprised between 0.9 and 1.1, although it can be locally as low as 0.6. At the location selected for the observations of Figure 6a-c, it is close to 1.1.

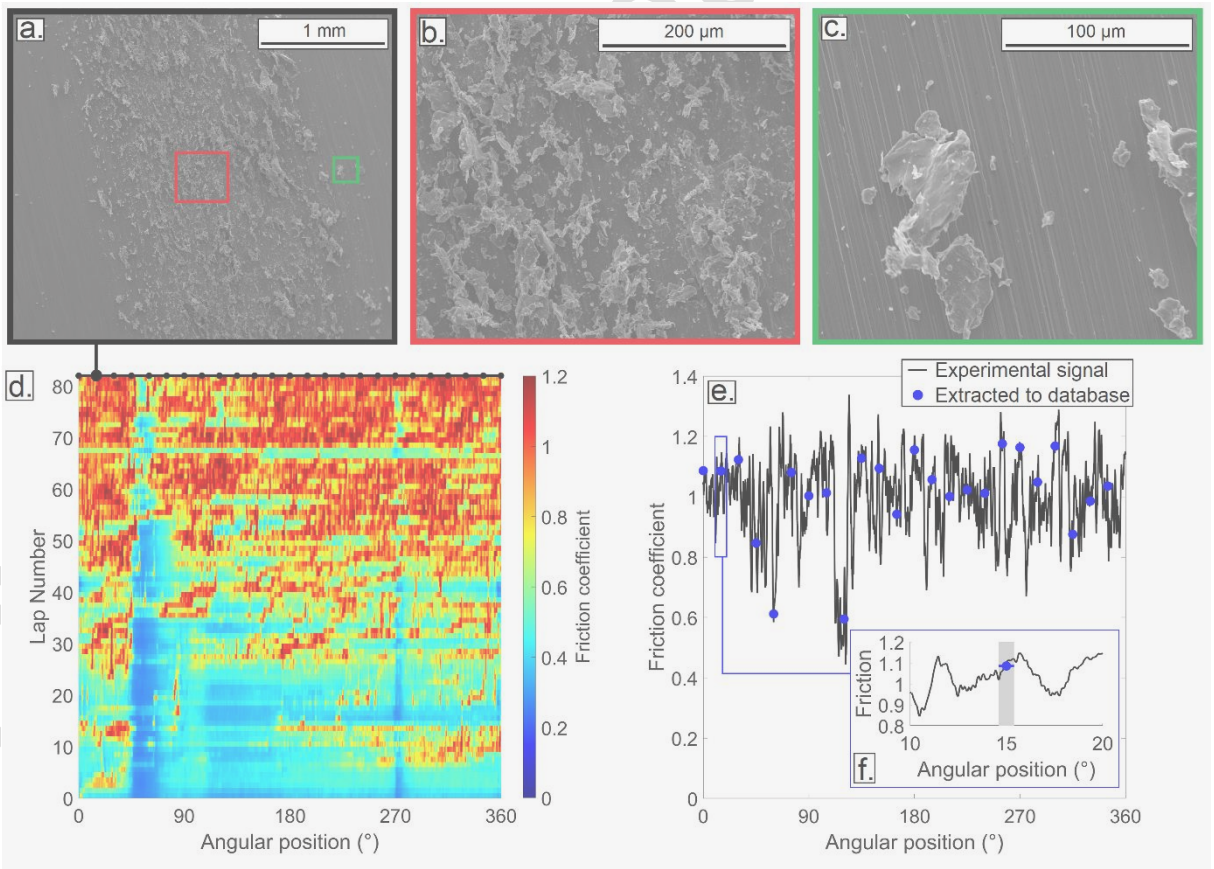

Figure 6: Local observations and measurements for a long test in argon: D12P29. a. General view of the track after 85 laps at the angular position 15°; b. View of the centre of the track; c. View of the ejection zone (exterior); d. Friction map with black dots indicating SEM observations (including a., b., c.); e. Friction signal during the last lap, with blue dots indicating SEM observation points extracted to the general database; f. Zoom on the friction averaging window around angular position 15°

2.4 Data extraction

Figures 4, 5, and 6 indicate that, despite (i) the limited number of test variables and (ii) the first body material is the same for all tests, the measured friction coefficient and the observed third body morphology at the end of each test do vary a lot. We may therefore wonder whether a strong quantitative link may be established between these two classes of observations. The main question would be: “Is the value of the instantaneous friction coefficient coded in the aspect of the friction track described in the previous section?”. Establishing such a link is a typical task for machine learning, as we elaborate later, but it requires to first extract relevant quantitative data from the raw experimental results. To that end, regions of interest (ROI) are sampled every θ=15° on the wear track (figure 2) of each of the 14 experimental tests, giving a total of 336 ROI. For each ROI three images are taken: one of the center of the track and two of its sides (Figure 2). These two categories of images, highlighting different third body morphology, have to undergo different processing techniques in order to extract features, also called descriptors.

Because of their complexity and of the large concentration of third body at those locations, the track centre images are treated as textures for which co-occurrence matrices must be calculated. From these matrices it is then possible to evaluate various descriptors such as homogeneity, contrast, (informational) entropy, energy, ASM, correlation and dissimilarity. As detailed in [25], these quantities can be related in a statistical way to such morphological properties as the complexity or the heterogeneity of the third body layer aspect. These descriptors reflect the morphology of third body due to the internal flow (Q_i).

In contract, the wear flow (Q_w) is described by the morphology of the ejected particles in the two lateral regions of each ROI, where the particles are more scarce and easier to characterize individually. To achieve this, the images of track sides must be segmented to access this information. The diversity of third body particles presented in the previous section prevents the use of so-called "classical" segmentation methods (i.e., based on thresholding or edge detection [22], [26], [27]. To overcome this, we developed a semi-automatic segmentation program based on machine learning, whose operation is described in detail in a previous work [25]. In this program, each pixel of the image to be processed is defined by a set of grey level values, evaluated based on geometric reconstruction and texture characteristics. This set of values is processed by a neural network that has been trained to classify pixels as "part of a particle" and "not part of a particle". Once the images have been segmented, 21 descriptors can be measured, divided into three categories: number of particles, size (including

perimeter, area, convex area.) and shape (including circularity, roundness, Minkowski metrics [28], elongation, aspect ratio, solidity, extend and equivalent diameter). At the end of this image analysis processing phase, 7 texture descriptors and 21 particle descriptors are available for each ROI (center, interior and exterior). In several cases, explained later in section 3.2, these descriptors could be reduced to statistical descriptors like average and standard deviation.

Finally, each ROI is associated with a friction coefficient value. This is done by extracting this value from the friction measurements during the last lap of each test (e.g., Figures 4e, 5e, 6e), every 15° on the track. To account for the fact that the ROI have a certain spatial extension, a local averaging of the raw friction signal is performed over the corresponding time window (e.g., Figures 4f, 5f, 6f).

A histogram of the friction coefficients extracted at the 336 ROI is provided in Figure 7. It shows that the measured value covers the whole range of typical values for dry friction (i.e., from ~0.1 to ~1.3), with a larger concentration of values in the range 0.6-0.8. This figure also shows that tests in argon generally lead to larger friction coefficients (especially long ones, which constitute all the cases for which friction is larger than 1), while the tests in ambient air are generally less frictional (especially short ones, which constitute all the cases for which friction is lower than 0.3).

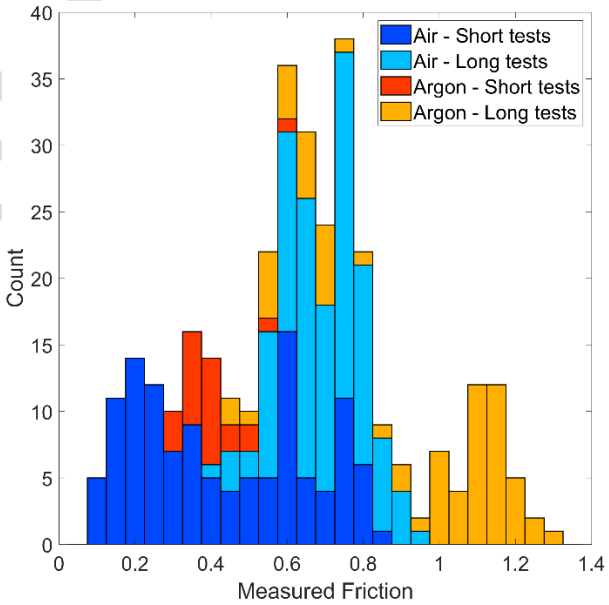

Figure 7: Histogram of the local friction measurements in the database, colour-coded by test environment and duration. The threshold between short and long tests is put at 10 meters of sliding.

An important point to notice is that, in this work, the morphology of the pin is completely disregarded. Indeed, the pin surface morphology cannot be directly associated with a given location on the track and with a given value of the friction coefficient. Despite its important role in the tribosystem, the pin therefore cannot bring any relevant information in the present context.

3. Machine Learning

3.1. Machine learning algorithm

Among the numerous existing ML algorithms, random forest (RF) was chosen in the present study, essentially for three reasons:

1. With an equivalent model, it has a more reasonable computation time than comparable algorithm, like Multi-Layer Perceptron (MLP) or Support Vector Machine (SVM). Thanks to the parallelization of the computations [29], [30]. This feature, although not negligible for large models, is not essential here.
2. Because of its nature as an ensemble method, the random forest makes it possible to work with small databases with a large dimension, i.e., a small number of samples but a large number of features [30], [31].
3. Finally, this algorithm could evaluate the influence of features during the learning and prediction processes [32].

Before presenting the Random Forest (RF) algorithm used in this study it is necessary to introduce the concept of a decision tree. A decision tree initially consists of a root node containing all the observations in the learning database. Classically, this node will divide into 2 children nodes using a separation rule chosen according to the task allocated to the tree. Examples of rules and how they work are described in [29], [30], [33]. This division is then repeated until the leaves are obtained, which are the lowest levels of the tree. The depth (i.e. number) of these levels can be parameterized using the model's hyperparameters.

Alternatively, we can say that the algorithm separates the training set into two subsets using a single feature k and a threshold tk. It searches for the pair (k, tk) that minimises the mean square error (MSE) weighted by the size of the subsets. The process is applied recursively to the subsets and stops when the maximum depth is reached (max_depth hyperparameter) or when there are no more features reducing the square error [30], [32]. Gerard Biau [32] proposes a simple definition of this concept: "decision trees are tools for recursively slicing space with local decision-making". Empirically, it has been observed that a different decision rule could have been chosen at each stage of tree construction. To compensate for this phenomenon, it is possible to build a collection

of trees called a forest, thus overcoming the instability of the predictions of a single tree. Another virtue of this method is that it reduces the complexity of the problem, as each tree in the forest will be required to process less data [32]. This sampling will also make it possible to set aside data not used to build the trees, which will be used for variable selection.

To use a machine learning algorithm, the user must adjust the hyperparameters. Thus, as demonstrated by [31], [34], the significant hyperparameters of a random forest are:

- n-estimators: Number of trees in the forest.
- max-depth: Maximum tree depth. If None, nodes are developed until all leaves are pure, or until all leaves contain less than min-samples-split samples.
- min-samples-split: The minimum number of samples required to split an internal node.
- max-features: The number of features to be considered when search for the best division.

When it comes to adjusting (also known as tuning) hyperparameters, several steps should be followed. The first is to determine which hyperparameters have the greatest influence. This can be done empirically, by varying the parameters in turn[31], [34]. Sensitivity analysis methods such as Morris' method [35], genetic algorithms (GA) or Tagushi's experimental design [36], [37] can also be used to select the parameters to be adjusted. Once the relevant hyperparameters have been selected, two tools developed in the scikit-learn Python librairy can be used: RandomizedSearchCV and GridSearchCV. Starting with GridSearchCV, the user creates a grid of parameters to test, then defines a blank model to train. The GridsearchCV method then tests all available hyperparameter combinations and proposes the best performing one. This method is particularly suited to cases where the number of parameters to be tested is small. If the search space is large, it is preferable to use RandomizedSearchCV [30]. Instead of trying all possible combinations, it evaluates a user-defined number of cases. At each iteration, the method selects a random value for each hyperparameter until a satisfactory convergence is achieved.

Due to its low computational cost and widespread use in the domain, Python has been chosen as the programming language. The scikit learn python library [38] is chosen to implement the Machine Learning algorithm. The program is developed as a python notebook and follows a number of 5 steps. The figure 8 presents a schematic workflow to illustrate its operation. At the end of the process the trained forest is saved in a binary file to be able to reuse it later.

Figure 8: Workflow of machine learning processing

Several metrics exist to measure the predictive ability of an algorithm. The most classical is the coefficient of determination R^2 but it is not the most adapted to multivariate regression problems because it is very sensitive to extreme values [30]. This is why the average error on the predictions is calculated, named ErrMean and defined as:

$$ErrMean = \frac{|y_{pred} - y_{measured}|}{nb_{measures}}$$

The average error is very dependent on the way the training and test sets are split. To remove the randomness linked to this operation, the cutting procedure can be reproduced several times and average the performances obtained. This is called Crossed Validation, and the performance is evaluated by calculating the root mean square error called CVscore. The CVscore is computed for ten successive cuttings, that allows to avoid overfitting. The results for each database are computed on the whole test sets. This type of validation allows us to be statistically representative.

3.2. Candidate databases

The next step is the construction of a database (DB) to be fed into a ML algorithm. Regarding friction prediction from morphological data, this approach was initiated by [22] and is seldom used in tribology. To be as exhaustive as possible, four databases are therefore built, as summarized in Table 2. They are representative of several approaches and are built from the first eight tests (D10P20 to D10P27) presented in the Table 1. The nomenclature of each database gives an information relative to its content: the keyword "*part*" is related to

individual particle descriptors, "*partStat*" is related to the statistical first moments of the particle descriptors (and thus to the wear flow) and finally "*text*" refers to the texture descriptors (and thus to the internal flow).

Designation	Number of samples	Number of features/sample	Content
DBpart	7354	21	Descriptors of each particle at each angular position. Local study of the wear flow (Q_e).
DBpartStat	192	84	First statistical moments of the particle descriptors at each angular position + number of particles. Global study of the wear flow (Q_e).
DBtext	192	7	Texture descriptors at each angular position. Study of internal flow (Q_i).
DBtextPartStat	192	91	Texture descriptors + First statistical moments of the particle descriptors at each angular position + number of particles. Study of the internal flow (Q_i) with consideration of the wear flow (Q_e).

Table 2: Description of the databases (DB) built from the morphological characteristics of third bodies, from tribological tests D10P20 to D11P27: a sample corresponds either to one location ϑ (DBpartStat, DBtext, DBtextPartStat) or one particle (Dbpart).

3.3. Database selection

The hyperparameters fitting and training process is implemented for each of the databases detailed in Table 2, resulting in 4 binary files containing the four forests sized and trained. When establishing these performances, we did not face any case of suspected overfitting, so the metrics proposed in Table 3 are established on the test sets.

	DBpart	DBpartStat	DBtext	DBtextPartStat
ErrMean	0.1644	0.1540	0.1318	0.1363
CVscore	0.2068±0.017	0.2243±0.08	0.2101±0.102	0.1978±0.05

Table 3: Performances metrics of RF evaluated on test sets (tribological tests D10P20 to D11P27)

Not all databases are equal in terms of predictive power, and a joint study of performance metrics is required in order to choose the database containing the most relevant information. The DBpart database is first evaluated given its ”historical” status. Indeed, in the literature, it is from the morphological characteristics of the particles that it is possible to trace back the test conditions or the wear mechanisms [4], [6], [39]. The database *DBpart*, containing only individual particles, the average error seems at first sight to be of the same order as the others, but plotting the predicted value of the COF against the measured value reveals important deviations (Figure 9a).

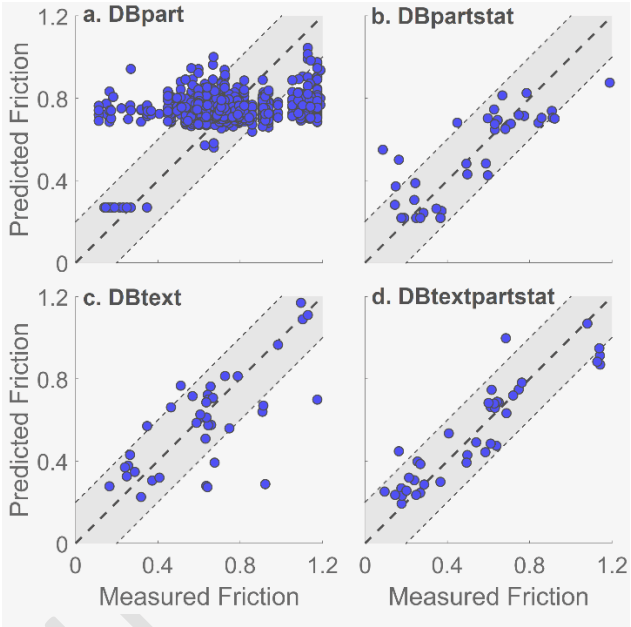

Figure 9: Comparison of the measured and predicted friction value from the test sets of the databases DBpart - DBtext - DBpartStat - DBtextPartStat. Bold dotted lines correspond to measure = prediction, grey areas correspond to a prediction error lower than 0.2.

The model most often predicts a value close to 0.7, the base being composed of 4 tests in running-in (presenting little particle ejection) and 4 tests in established regime with a significant increase in the number of particles up to 100 attributed to the same friction coefficient. It appears that the friction coefficient associated with the presence of a particle is assimilated to the asymptotic value of friction observed on Figure 3. This observation is consistent with our lack of knowledge about the moment of creation and ejection of the particles. As a consequence, it seems incongruous to attribute the friction value measured during the last lap of the test to a particle ejected at an unknown time of the test. That is in good agreement with previous findings [22], [39] .

Disregarding individual particles and focusing on the whole wear flow, it is envisaged in a second time to average the values and to count the particles on their ejection site. It is in this perspective that the database *DBpartStat*

is built, because it contains the first statistical moments of the morphological descriptors of the particles in each site of measurement, as well as the number of particles at each angular position (Table 2). The results are much more satisfactory. The plot of predicted values versus measured values (Figure 9b) shows that, even though predictions are slightly inaccurate, the model leads to a greater variety of predicted values. The value of the average error is lower than for the database *DBpart* but does not find its source in the same mechanisms. Indeed, since the ejected particles are mainly present in the steady state and are assimilated to an asymptotic coefficient of friction, the absence of particle is not a lack of information but the indication that the wear flow is negligible. This suggests that there is information, albeit incomplete, about the friction coefficient in the overall wear flow.

In the first two cases presented, the *CVscore* is greater than 0.20 which is considered a high deviation for a friction coefficient measured in the range [0.1, 1.3]. Some information is therefore still missing for accurate prediction. This is why, in a third time, the focus is made on the internal flow and thus at the database *DBtext* which contains the texture descriptors related to the center of the wear track. In the case of *DBtext,* the quality of the prediction improves. The study of the associated graph (Figure 9c) shows predicted values closer to the measured ones, apart from a few outliers. The information related to the friction coefficient seems to be partly written in the morphology of the third body in the center of the track. The next logical step is to assess if it is possible to obtain even more information by combining the data related to the wear flow and those related to the internal flow. This is the purpose of the database *DBtextPartStat*, which contains both data on particles and textures.

The quality of the prediction for *DBtextPartStat* (Figure 9d) is similar to the one obtained for *DBtext*. This last database presents similar performances to *DBtext*, it is a little better with regard to *ErrMean*. A better way to compare these predictions is the *CVscore*, this metric is a good indicator of statistical stability. Moreover, the uncertainty is also lower, and the number of outliers is more limited. The database *DBtextPartStat* is therefore statistically more representative and allows to make more stable predictions. Thus, *DBtextPartStat* configuration is kept for the rest of the study.

3.4. Generalization test of the trained model

At the end of the performance evaluation, only *DBtextPartStat* is retained, along with the random forest trained on this basis. As this method has shown satisfactory results in training and testing, the question of generalization

arises. The data from the four trials tribological tests D12P28 to D12P31 are then used as a blind test, to evaluate the generalization capabilities of the trained model.

The particularity of these data is that they were produced using a 15mm thick disk, possibly slightly modifying the dynamic response of the tribosystem. The idea is to assess whether the model correctly generalizes on new data produced on a new disk with a slightly different geometry (which adds an extra difficulty). Analysis of the friction maps for two illustrative tests from the training and generalization databases presented in Figure 10 shows a relatively similar general trend for the 10 mmm and 15 mm thick disks, as observed in friction maps (Figure 10a-b), but higher friction coefficient values (by ~23%) for the 15mm disc (D12P31). The lap-by-lap history of contact shows more differences, with test D10P23 showing a period in the middle of life when friction drops sharply, as well as a noticeable space variability during the few last laps. An event clearly occurred between 40° and 120°. Test D12P31 has two areas of the disc with low friction coefficient, especially at the beginning of the test. Later in the test the friction becomes more uniform, despite a few local events leading to slight decreases in friction. These events may be attributable to a piece of the third body coming loose (from the pin or the disc) and being crushed on the track.

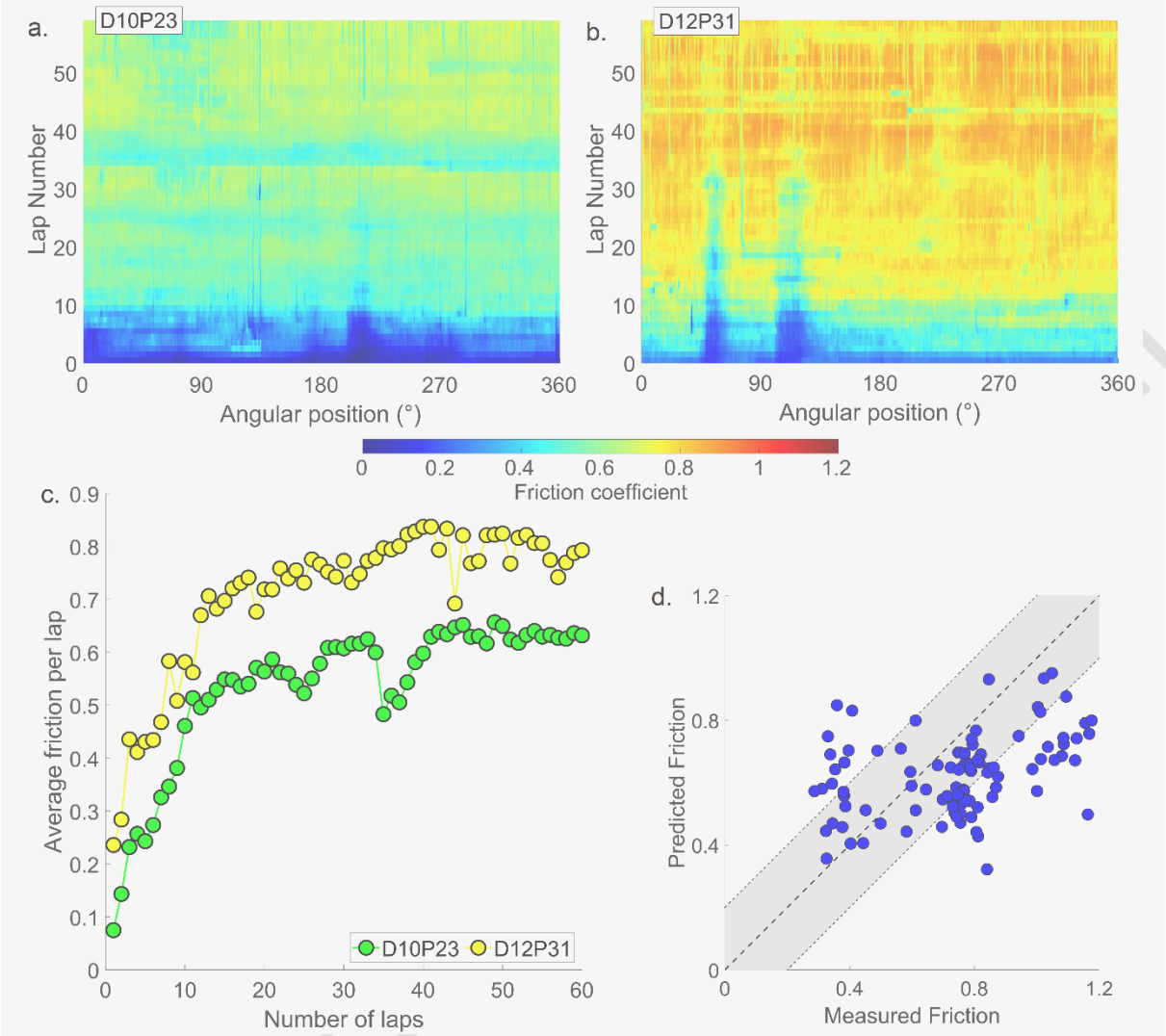

Figure 10: Generalization test for the model built on the DBtextPartStat database: a. Friction map for a typical test from the database used to train the model (test D10P23); b. Friction map for a typical test from the database used to blind-test the model (test D12P31); c. Friction histories for both tests; d. Comparison of measured and predicted friction values for tests on 15 mm-thick discs (D12P28 to D12P31) after training on 10 mm-thick discs (D10P20 to D11P27). Bold dotted line corresponds to measure = prediction, grey area corresponds to a prediction error lower than 0.2.

The generalization test leads to the following metrics: *ErrMean* = 0.2143; *CVscore* = 0.1937 ± 0.1306. In fact, Figure 10d shows very fragmented values around the straight-line *Measured Values* = *Predicted Values.* The average prediction error of 0.2143 is much larger than during the test phase of the initial DBtextPartStat database, and in terms of the *CVscore* the prediction is not stable. Very few significant differences in term of prediction were expected given the small variation in thickness, but it turned out that this modification of the mechanical system makes it difficult for the algorithm to predict the friction coefficient. This significant difference needs to be taken into account when creating the database, which needs to be upgraded to make it more versatile.

4. Database improvement and discussion

As previously explained, the model trained on data from 10mm-thick discs does not allow generalization to data produced from a different mechanical system (15mm-thick disc). This certainly indicates that the model did not meet a sufficient variety of situations during training. To overcome this problem, a new database is built from the data produced on the first 12 tests (D10P20 to D12P31) involving 10mm and 15mm disks, and the value tables are concatenated and randomly shuffled. The new database thus obtained is named *DBmix* and includes 288 samples characterized by 91 features and labelled by their corresponding friction coefficient. This database is divided into a training set (80%) and a test set (20%), then the RF is optimized using the tools presented in Section 3.1. Table 4 shows the optimal hyperparameters of the RF.

Hyperparameter	Value
n-estimators	1200
n-samples-split	2
n-samples-leaf	1
max-features	'auto'
max-depth	None
Bootstrap	True

Table 4: Optimized hyperparameters for DBmix treatment

The tuned forest is trained and saved, its performance on the test set is as follows:

- *ErrMean* = 0.1382
- *CVscore* = 0.1806 ± 0.0476

The *ErrMean* and *CVscore* for the latter are similar or even better than for *DBtextPartstat* presented in Table 3. The comparison between the measured and predicted values for the training and test sets is provided in Figure 11a (respectively the black and blue round dots). The predictions are generally satisfactory, with a majority of points located near the measure = prediction diagonal, despite a few outliers. The high measured values (when > 0.8) however seem to be systematically under-predicted. This feature could already be observed in the previous database *DBtextPartStat* and is true both for the training and the test sets. It is therefore not the result of overfitting, but more likely an inherent limitation of the RF or of the database. In Figure 11b, the predictions made for tests in air are relatively satisfactory, whereas tests in argon are the source of larger prediction errors. During long tests under argon, the COF value often tends to be underestimated, whereas for short tests corresponding to smaller COF values (of the order of 0.4) the predictions are usually overestimated (see for example the first

column of Figure 12). Since these errors are mainly due to Argon tests, this suggests that some information is lost or distorted when the third body descriptors are extracted. One possible explanation for this phenomenon is the orientation of the particles. When the third body produced under Argon is observed, the particles may be oriented vertically. A particle present in the form of a flake in 3D appears in the image (in 2D) as a more or less long filament, so descriptors such as area will be minimized in favor of others such as elongation, thereby introducing an error in the characterization of the morphology of the third body.

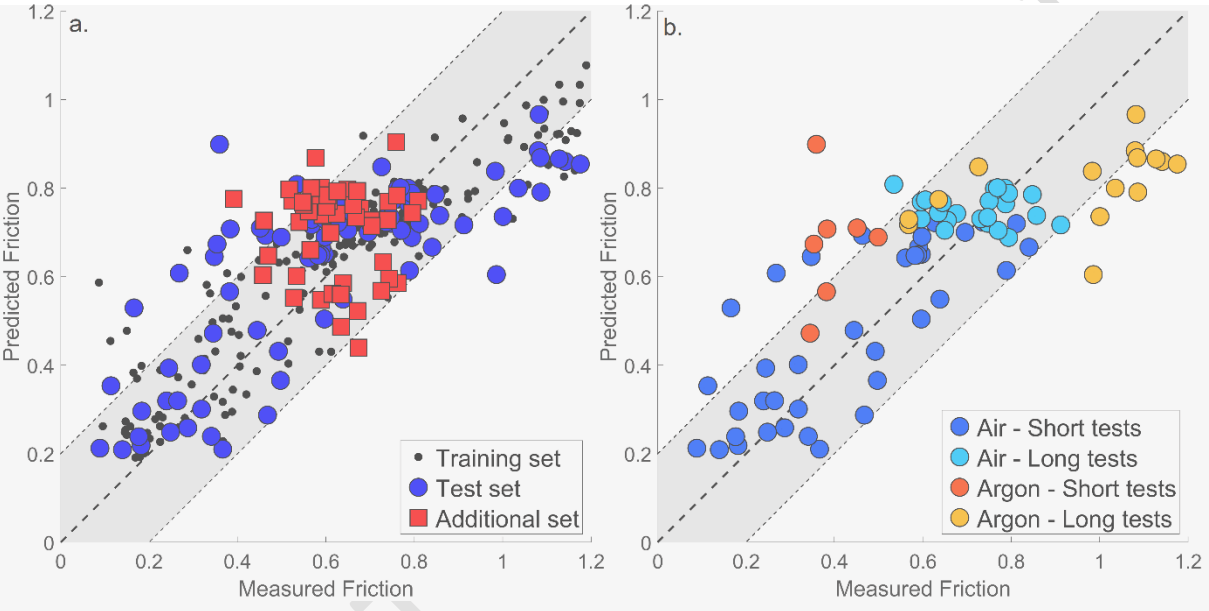

Figure 11: Comparison of measured and predicted COF values from DBmix. a. Predictions for the training set, the test set, and the additional set; b. Predictions for the test set only, with colors indicating environment and test duration. Bold dotted lines correspond to measure = prediction, grey areas correspond to a prediction error lower than 0.2.

These results are more satisfactory than those presented in Figures 10d but required to use the data initially conserved to test the generalization of the model. The ability to generalize will therefore be tested on the additional tests realized on two untested 10 mm- and 15 mm-thick discs (D17P42 and D151P43 respectively), in ambient air and for a sliding distance of 25m (Table 1). The characteristics of the third body produced during these tests are then evaluated by the model trained on *DBmix* and give the following results:

- *ErrMean* = 0.1438
- *CVscore* = 0.0882 ± 0.0371

The Figure 11a shows that the measured friction values are all within the interval 0.4 – 0.8, which is not very wide when compared to the typical prediction error. This can be explained by the nature of the tests, which are two steady-state tests under free atmosphere. This leads to a bulky cloud of points (red squares), despite the fact that

the prediction error is only slightly larger than for the test set (0.1438 instead of 0.1382). In addition, the low value of the *CVscore* indicates a good stability of this prediction error. Overall, these results are very encouraging, and demonstrate a clear ability of the trained model to provide acceptable predictions on the friction coefficient between two bodies unseen by the training set.

The creation of *DBmix* has therefore improved the model's ability to generalize. However, the prediction error remains higher than the error evaluated on the test set, which can be explained by the variability of the experimental results. Indeed, as shown in Figure 3, the tests show a common trend but a very distinct history. This history can be kept in memory in the third body, through a more or less important ejection flow or a more or less smoothed internal flow. These are all events that can render the input data noisier and thus introduce error into the prediction.

Figure 12 depicts the last lap of several selected experiments, along with measured and predicted (either during training, testing, or additional generalization) by the algorithm. As it stands, the trained algorithm is able to predict the coefficient of friction with an average error of ~0.14, despite the large range and the significant variability in the coefficient of friction. This result is quite remarkable on its own, given the complexity and apparent unpredictability of local friction values as depicted in Figures 4, 5, and 6. It confirms that the friction coefficient of a given interface at a given location is strongly related to the local properties of the third body [23], [24], and that a part of the information regarding friction is coded in its morphological aspect. In addition, this predictive ability proves to be generalisable, with the same quality, on new experimental data (carried out under air, Figure 11 and 12). The prediction for the Argon tests seems more complicated (Figure 12), as the friction is highly variable for morphologically similar types of third body. These tests were kept in the databases for two reasons: they noised the data, thereby limiting overfitting, and they represent the first step in enriching the database with new experimental conditions and new third body morphologies. As mentioned above, the orientation of particles produced in Argon tends to distort predictions, so it may be worth looking for one or more descriptors to account for this effect. It should be noted that increasing the database with just two tests noticeably improved its performance, which can only incite to enrich it with more data produced under similar conditions.

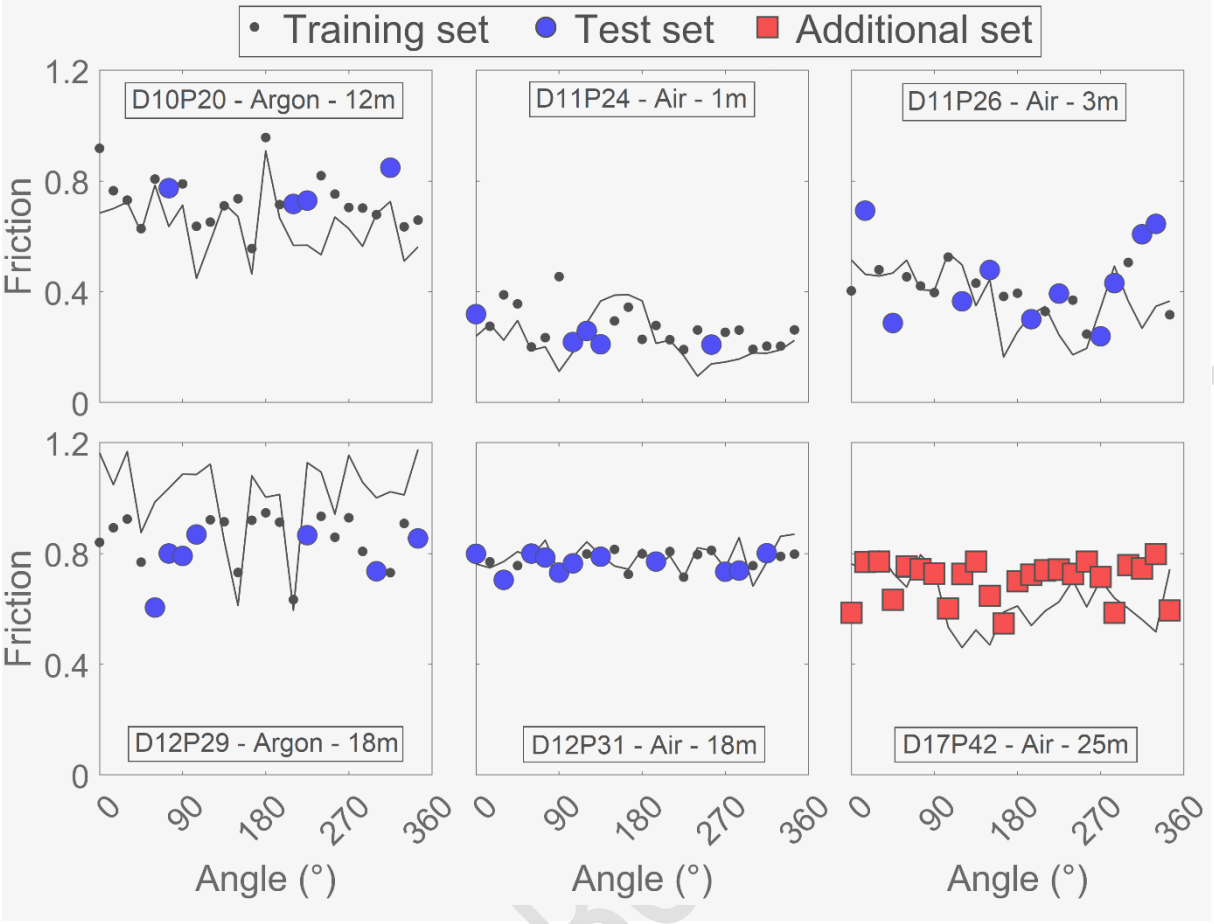

Figure 12: Last friction lap for six selected tests, comparing measured and predicted (either during training or during test) local friction values at the sampling points every 15°

5. Conclusion

In this study, twelve tribological tests were performed on steal-steal pin-on-disc tribopairs, varying three operating parameters: atmosphere, duration, and disk thickness. These tests were supplemented by systematic SEM image acquisition, which allowed to directly associate an instantaneous friction coefficient and a third body morphology. Based on the collected experimental data, five different databases were built focusing on various morphological components, in order to gain knowledge on the best way to collect such morphological data. For this purpose, Machine Learning algorithms was trained to predict instantaneous friction from these databases. Results demonstrated that the content of of data base can influence the prediction of friction: The best predictions were obtained while combining information relative to (i) statistics of the morphology of the particles ejected from the track and (ii) textural properties of the third body layer lying on the wear track. These predictions achieved a surprisingly high level of accuracy (average error of ~0.14 on the friction coefficient, while the

measured values ranged from ~0.1 to ~1.2), and it is likely that this accuracy could be greatly improved by increasing the size of the database and exploring the performances of other classes of ML algorithms.

Another promising research avenue would be to focus on the explicability of the trained model, in order to gain knowledge about the process it uses to make its predictions. This can only provide relevant tribological knowledge about the structural, mechanical, physical, and chemical phenomena which control instantaneous friction. Also, despite the random forest's ability to work on databases with a large number of features, it would first be interesting to reduce this number in order to make the model more explainable. This work on reducing the number of features and the search for model explicability will be the subject of a future study. Notwithstanding the likely improvements that may be obtained in the future thanks to these refinements, this work provides a solid and quantitative proof that a direct link exists between third body morphology and instantaneous friction. It must encourage the tribological community to keep exploring this link in order to improve our understanding and prediction of dry friction in three-body contacts.

Credit authorship contribution statement

Alizée Bouchot: investigation, Software, Methodology, Writing - original draft.
Amandine Ferrieux: technical support
Johan Debayle: Conceptualization, Supervision, Writing - review & editing.
Guilhem Mollon: Conceptualization, Supervision, Writing - review & editing.
Sylvie Descartes: Conceptualization, Supervision, Project administration, Funding acquisition, Writing - review & editing.

Aknowledgements

This work has been funded by a public grant from the French National Research Agency (ANR) under the “France 2030” investment plan, which has the reference EUR MANUTECH SLEIGHT - ANR-17-EURE-0026

5.References

[1] Y. Chung and Q. J. Wang, *Encyclopedia of tribology: With 3650 Figures and 493 Tables*. Springer, 2013.
[2] M. Godet, “The third-body,” *Wear*, vol. 100, pp. 437–452, 1984.
[3] Y. Berthier, “Third-Body Reality - Consequences and Use of the Third-Body Concept to Solve Friction and Wear Problems,” Jan. 2005, doi: 10.1002/9780470017029.ch12.
[4] C. Kowandy, C. Richard, and Y. M. Chen, “Characterization of wear particles for comprehension of wear mechanisms. Case of PTFE against cast iron,” *Wear*, vol. 265, no. 11–12, pp. 1714–1719, 2008, doi: 10.1016/j.wear.2008.04.036.
[5] C. Kowandy, C. Richard, Y. M. Chen, and J. J. Tessier, “Correlation between the tribological behaviour and wear particle morphology-case of grey cast iron 250 versus Graphite and PTFE,” *Wear*, vol. 262, no. 7–8, pp. 996–1006, 2007, doi: 10.1016/j.wear.2006.10.015.

[6] B. J. Roylance and S. Raadnui, “The morphological attributes of wear particles - their role in identifying wear mechanisms,” *Wear*, vol. 175, no. 1–2, pp. 115–121, 1994, doi: 10.1016/0043-1648(94)90174-0.

[7] G. Wang *et al.*, “Tribological performance study and prediction of copper coated by MoS2 based on GBRT method,” *Tribol Int*, vol. 179, p. 108149, 2023, doi: https://doi.org/10.1016/j.triboint.2022.108149.

[8] A. T. Sose, S. Y. Joshi, L. K. Kunche, F. Wang, and S. A. Deshmukh, “A review of recent advances and applications of machine learning in tribology,” *Physical Chemistry Chemical Physics*, 2023.

[9] P. M. Sieberg and S. Hanke, “Challenges and potentials in the classification of wear mechanisms by artificial intelligence,” *Wear*, vol. 522, p. 204725, 2023.

[10] M. Marian and S. Tremmel, “Current trends and applications of machine learning in tribology—a review,” *Lubricants*, vol. 9, no. 9. MDPI, Sep. 01, 2021. doi: 10.3390/LUBRICANTS9090086.

[11] M. S. Hasan, A. Kordijazi, P. K. Rohatgi, and M. Nosonovsky, “Triboinformatic modeling of dry friction and wear of aluminum base alloys using machine learning algorithms,” *Tribol Int*, vol. 161, p. 107065, 2021, doi: https://doi.org/10.1016/j.triboint.2021.107065.

[12] A. Halevy, P. Norvig, and F. Pereira, “The unreasonable effectiveness of data,” *IEEE Intell Syst*, vol. 24, no. 2, pp. 8–12, 2009.

[13] D. Nowell and P. W. Nowell, “A machine learning approach to the prediction of fretting fatigue life,” *Tribol Int*, 2020, doi: 10.1016/j.triboint.2019.105913.

[14] N. Motamedi, V. Magnier, and H. Wannous, “Towards the identification of the link between the contact roughness and the friction-induced vibration: Use of deep learning,” *European Journal of Mechanics - A/Solids*, vol. 99, p. 104949, 2023, doi: https://doi.org/10.1016/j.euromechsol.2023.104949.

[15] M. Di Bartolomeo, F. Massi, L. Baillet, A. Culla, A. Fregolent, and Y. Berthier, “Wave and rupture propagation at frictional bimaterial sliding interfaces: From local to global dynamics, from stick-slip to continuous sliding,” *Tribol Int*, vol. 52, pp. 117–131, 2012.

[16] D. Tonazzi, F. Massi, L. Baillet, J. Brunetti, and Y. Berthier, “Interaction between contact behaviour and vibrational response for dry contact system,” *Mech Syst Signal Process*, vol. 110, pp. 110–121, 2018.

[17] Y. Berthier, “Maurice Godet’s Third Body,” in *The Third Body Concept Interpretation of Tribological Phenomena*, vol. 31, D. Dowson, C. M. Taylor, T. H. C. Childs, G. Dalmaz, Y. Berthier, L. Flamand, J.-M. Georges, and A. A. Lubrecht, Eds., in Tribology Series, vol. 31. , Elsevier, 1996, pp. 21–30. doi: https://doi.org/10.1016/S0167-8922(08)70766-1.

[18] N. Fillot, I. Iordanoff, and Y. Berthier, “Wear modeling and the third body concept,” *Wear*, vol. 262, no. 7–8, pp. 949–957, 2007.

[19] M. Renouf, F. Massi, N. Fillot, and A. Saulot, “Numerical tribology of a dry contact,” *Tribol Int*, vol. 44, no. 7–8, pp. 834–844, 2011.

[20] Y. Waddad, V. Magnier, P. Dufrénoy, and G. De Saxcé, “A new contact model for multilayered solids with rough surfaces,” *Tribol Lett*, vol. 65, no. 4, p. 155, 2017.

[21] O. Bouillanne *et al.*, “How vorticity and agglomeration control shear strength in soft cohesive granular flows,” *Granul Matter*, vol. 24, no. 2, p. 55, 2022.

[22] R. Jaza, G. Mollon, S. Descartes, A. Paquet, and Y. Berthier, “Lessons learned using machine learning to link third body particles morphology to interface rheology,” *Tribol Int*, vol. 153, no. May 2020, p. 106630, 2021, doi: 10.1016/j.triboint.2020.106630.

[23] Y. Zhang, G. Mollon, and S. Descartes, “Significance of third body rheology in friction at a dry sliding interface observed by a multibody meshfree model: Influence of cohesion between particles,” *Tribol Int*, vol. 145, p. 106188, 2020, doi: https://doi.org/10.1016/j.triboint.2020.106188.

[24] G. Mollon, “Solid flow regimes within dry sliding contacts,” *Tribol Lett*, vol. 67, pp. 1–20, 2019.

[25] A. Bouchot, A. Ferrieux-Paquet, G. Mollon, S. Descartes, and J. Debayle, “Segmentation and morphological analysis of wear track/particles images using machine learning,” *J Electron Imaging*, vol. 31, no. 5, p. 51605, 2022.

[26] Y. Gavet and J. Debayle, *Image processing tutorials with python*. Spartacus IDH, 2019.

[27] A. Bouchot, A. Ferrieux, J. Debayle, G. Mollon, and S. Descartes, “Image processing applied to tribological dry contact analysis,” *Wear*, vol. 476, no. December 2020, p. 203748, 2021, doi: 10.1016/j.wear.2021.203748.

[28] F. M. Schaller, J. Wagner, and S. C. Kapfer, “papaya2 : 2D Irreducible Minkowski Tensor computation,” vol. 5, pp. 4–8, 2020, doi: 10.21105/joss.02538.

[29] C. A. Azencott, *Introduction au machine learning*. Dunod, 2018.

[30] A. Géron, *Hands-on machine learning with Scikit-Learn, Keras, and TensorFlow*. " O'Reilly Media, Inc.," 2022.
[31] R. Genuer, J.-M. Poggi, and C. Tuleau-Malot, "Variable selection using random forests," *Pattern Recognit Lett*, vol. 31, no. 14, pp. 2225–2236, 2010.
[32] G. Biau, "Analysis of a random forests model," *The Journal of Machine Learning Research*, vol. 13, pp. 1063–1095, 2012.
[33] S. Raschka, *Python machine learning*. Packt publishing ltd, 2015.
[34] E. Scornet, "Tuning parameters in random forests," *ESAIM Proc Surv*, vol. 60, pp. 144–162, 2017.
[35] M. D. Morris, "Factorial sampling plans for preliminary computational experiments," *Technometrics*, vol. 33, no. 2, pp. 161–174, 1991.
[36] S. Ansari, K. A. Alnajjar, S. Abdallah, M. Saad, and A. A. El-Moursy, "Parameter Tuning of MLP, RBF, and ANFIS Models Using Genetic Algorithm in Modeling and Classification Applications," in *2021 International Conference on Information Technology (ICIT)*, IEEE, 2021, pp. 660–666.
[37] Z. Guo, L. Xu, and N. Ali Asgharzadeholiaee, "A homogeneous ensemble classifier for breast cancer detection using parameters tuning of MLP neural network," *Applied Artificial Intelligence*, vol. 36, no. 1, p. 2031820, 2022.
[38] F. Pedregosa *et al.*, "Scikit-learn: Machine learning in Python," *the Journal of machine Learning research*, vol. 12, pp. 2825–2830, 2011.
[39] R. Jaza, "Prediction of the tribological behaviour of a contact with third body particles : Relating the morphological descriptors of the third body particles with the rheological parameters of the contact," 2020.